

1 **Avoidance of catastrophic structural failure as an evolutionary constraint:**
2 **Biomechanics of the acorn weevil rostrum**

3 M. Andrew Jansen,^{1,*} Jason Williams,² Nikhilesh Chawla,² and Nico M. Franz¹

4 ¹*School of Life Sciences, Arizona State University, Tempe, AZ 85287, USA*

5 ²*School for Engineering of Matter, Energy, and Transport,
6 Arizona State University, Tempe, AZ 85287, USA*

7 (Dated: May 19, 2019)

The acorn weevil (*Curculio* Linnaeus, 1758) rostrum (snout) exhibits remarkable flexibility and toughness derived from the microarchitecture of its exoskeleton. Here we characterize modifications to the composite profile of the rostral cuticle that simultaneously enhance the flexibility and toughness of the distal portion of the snout. Using Classical Laminate Plate Theory, we estimate the effect of these modifications on the elastic behavior of the exoskeleton. We show that the tensile behavior of the rostrum across six *Curculio* species with high morphological variation correlates with changes in the relative layer thicknesses and orientation angles of layers in the exoskeleton. Accordingly, increased endocuticle thickness is strongly correlated with increased tensile strength. Rostrum stiffness is shown to be inversely correlated with work of fracture; thus allowing a highly curved rostrum to completely straighten without structural damage. Finally, we identify exocuticle rich invaginations of the occipital sutures both as a likely site of crack initiation in tensile failure, and as a source of morphological constraint on the evolution of the rostrum in *Curculio* weevils. We conclude that avoidance of catastrophic structural failure, as initiated in these sutures under tension, is the driving selective pressure in the evolution of the female *Curculio* rostrum.

The exoskeleton of Coleoptera (beetles) is a hierarchically structured, fibrous composite – characterized by variously arranged α -chitin (N-acetylglucosamine) nanofibrils that are embedded in a heterogeneous protein matrix [1–3]. Although α -chitin is brittle and strongly anisotropic, beetle cuticle is simultaneously rigid and tough due to its unique laminate microstructure (reviewed in [4–6]), characterized in detail below. Impact-prone areas and exaggerated structures in arthropods generally exhibit cuticle organization that resists deformation and fracture [7–11]. However, acorn weevils in the genus *Curculio* Linnaeus, 1758¹ (Curculionidae in the sense of [13]) instead exhibit unusual distal flexibility in an elongate extension of the head called the rostrum (snout) [1, 14–16]. The rostrum is a hollow, strongly curved (over 90° in some species), cylindrical, exoskeletal extension of the otherwise nearly-spherical head, which bears at its apex the terminal chewing mouthparts [16–20]. This structure is used by the female to feed on fruit (plant) tissue and to excavate sites for egg-laying (oviposition, see Fig. 1). The rostrum can be repeatedly bent, without evident damage, and despite being composed of the same material as other rigid body parts [1, 14–16]. By maintaining constant pressure on the snout and rotating around the bore-hole, females are able to flex the rostrum into a straightened configuration and produce a linear channel into the fruit.

³⁴ A single adult female may prepare hundreds of such sites
³⁵ [15, 21, 22].

³⁶ Despite its documented performance in many *Curculio* species [15, 16, 21, 22], it remains unknown how the rostrum of female acorn weevils can withstand the repeated, often extreme bending incurred during the process of egg-chamber excavation. In this study, we therefore characterize the composite profile of the rostral cuticle to account for the observed flexibility of the snout. We show that the relative layer thicknesses and fiber orientation angles of the exocuticle and endocuticle of the rostrum are strongly differentiated from the head capsule and other body parts. The effect of these differences on the elasticity of the cuticle is estimated using Classical Laminate Plate Theory (CLPT). Recent studies have shown that the yield strength of the beetle exoskeleton is lower in tension than compression [23]. To assess the validity of these findings, we compare the ultimate tensile strength of the rostrum across species and snout morphotypes. We also report displacement-controlled load cycling results for the snout of one *Curculio* species with strongly curved morphology. Our results indicate that an increase in the volume fraction of endocuticle in the rostrum conveys higher tensile strength at the rostral apex across all tested species; and further, that a strongly curved rostrum can be flexed repeatedly without harm to the structure.

⁶⁰ Accordingly, the flexibility and tensile strength of the rostrum appear to be derived *exclusively* from modification of the composite architecture of the exoskeleton.
⁶¹ This is the first time that a modified composite profile has been reported as a means of enhancing structural elasticity in the insect exoskeleton (though see [24]). We additionally describe the fracture mechanics of the snout, while considering how modification of the cuticle may prevent crack formation during oviposition, particularly

* corresponding author, email: majanse1@asu.edu

¹ Pursuant to the International Code of Zoological Nomenclature, the first mention of any specific epithet will include the full genus and species names as a binomen (two-part name) followed by the author and date of publication of the name. This is not an in-line reference; it is a part of the name itself and refers to a particular act establishing the validity and fixing the identity of the corresponding name by that author [12].

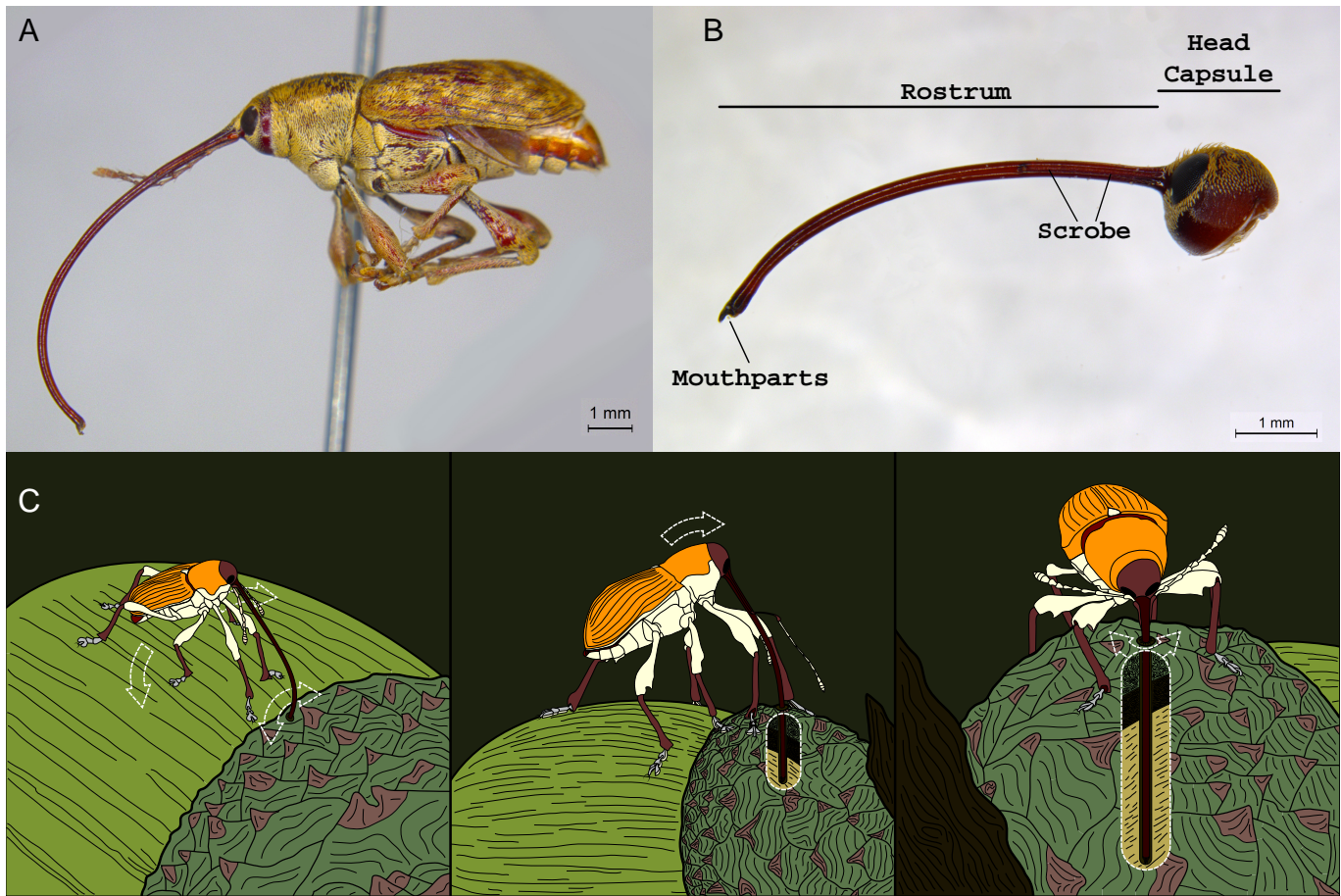


FIG. 1. Morphology and oviposition behavior of female *Curculio* weevils. **a**, Lateral habitus image of female *Curculio sayi* (Gyllenhal, 1836) featuring the elongate, strongly curved rostrum. **b**, Lateral view of head of female specimen of *Curculio longinasus* Chittenden, 1927, with major anatomical features indicated. **c**, Illustration of oviposition behavior, proceeding from left to right: female makes incision in host fruit, flexes head directly over bore-hole using front legs, then maintains tension on snout while rotating to excavate linear channel into fruit. During this process, female rostrum is bent until completely straight.

in the fracture-prone and exocuticle-rich occipital sulci.
Based on these findings we conclude that avoidance of catastrophic structural failure is the primary selective pressure in the evolution of the female *Curculio* rostrum.

I. MICROSTRUCTURE OF THE CURCULIO ROSTRUM

In arthropods – including beetles – the exocuticle is comprised of numerous unidirectional laminae of chitin nanofibrils. Each layer is the thickness of a single fiber (2–4 nm) embedded in a proteinaceous matrix [25, 26]. These layers are stacked at a more or less constant angle to each other, forming a quasi-isotropic laminate known as the Bouligand structure [6, 27, 28]. This layout effectively mitigates the strong anisotropy of α -chitin, thus yielding a versatile building material for the exoskeleton [2, 25, 26, 29]. Beetle endocuticle, however, is unique among arthropods and is comprised of large – 1–5 μm

diameter in *Curculio* – unidirectional bundles of chitin, called macrofibers. Chitin macrofibers are orthotropic (axial: $E_1 = 8.5 \text{ GPa}$; transverse: $E_2 = E_3 = 0.52 \text{ GPa}$ [1]), and arranged in unidirectional plies, as depicted in Figs. 2, 3 [4, 5]. Typically, adjacent macrofiber laminae are paired and pseudo-orthogonal – i.e., angled nearly 90° to each other (see Fig. 3; [30]) – with a constant stacking angle between pairs, although other configurations have been observed [3–5, 31]. This geometric sequence of the macrofiber laminae yields an approximately transversely isotropic composite, similar to the Bouligand structure [5, 26]. Notably, the resulting laminate is less rigid than the exocuticle, but exhibits greater toughness because the pseudo-orthogonal plies effectively inhibit crack formation and propagation between successive layers [3–5].

Serial thin sectioning and scanning electron microscopy of fractured *Curculio* specimens reveals that endocuticle in the head capsule fits this general profile, with an angle of nearly 30° between successive pairs of pseudo-orthogonal plies. Additionally, in the head capsule, the

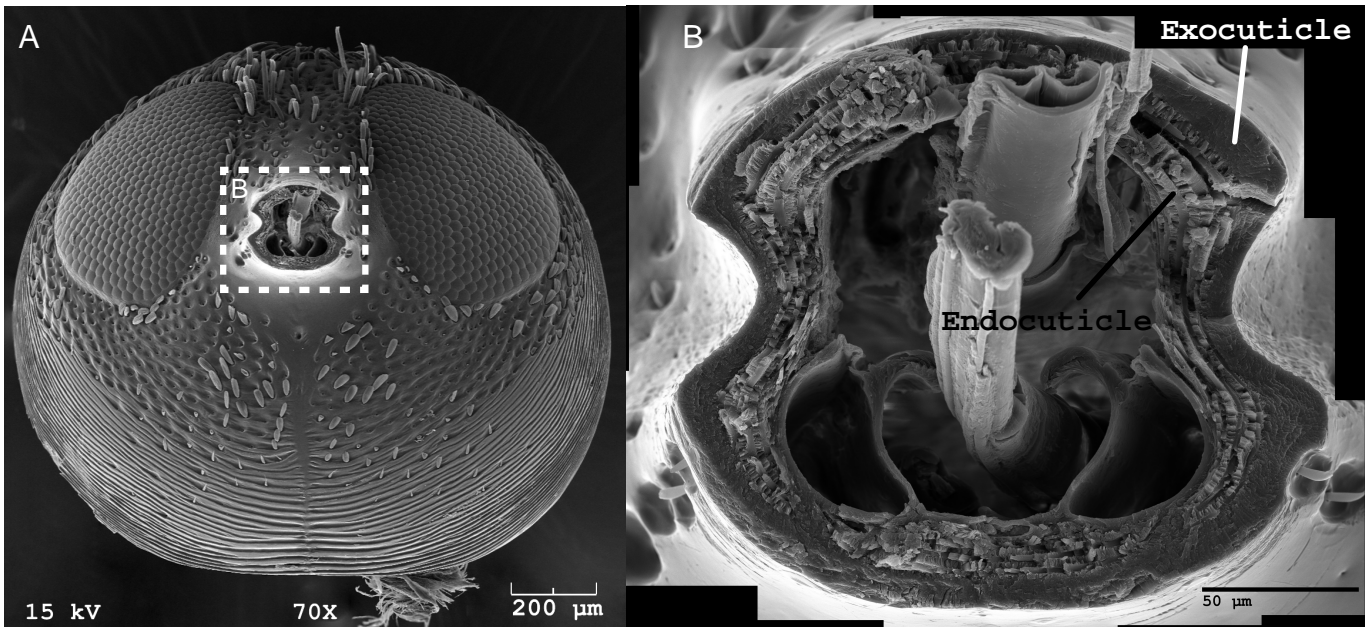


FIG. 2. Gross divisions of cuticle in the female *Curculio* rostrum. **a**, Scanning electron micrograph of head capsule, in frontal view, of female *Curculio sulcatus* (Casey, 1897), with rostrum removed. **b**, Magnified view of junction between rostrum and head capsule, showing division of cuticle into two general regions: exocuticle and endocuticle.

thickness of the exocuticle and endocuticle in cross-section is nearly equal – typically between 20–30 μm . However, the cuticle composite lay-up of the rostral apex is strongly differentiated from the head capsule, as shown in Fig. 3. Distally the exocuticle is reduced to a thin shell (ca. 5 μm), with the endocuticle thickened to offset this reduction and maintain a constant cuticle thickness (ca. 50 μm total) throughout its length. Moreover, the endocuticular macrofibers exhibit no rotation between successive pseudo-orthogonal plies; and are oriented at approximately $\pm 45^\circ$ to the longitudinal axis of the snout (i.e., an antisymmetric $[\pm 45^\circ]$ angle-ply laminate). We previously identified these modifications to the composite structure of the cuticle within a single species, *Curculio longinasus* Chittenden, 1927 [1, 14]. However, this composite profile is herein reported in the rostrum of six additional, phylogenetically disjoint, species, suggesting that this is an evolutionarily conserved trait throughout the genus *Curculio*. In all examined species, the portion of the snout between the head capsule and apex of the scrobe exhibits a gradual transition in composite profile along an anterior-posterior gradient.

Here we estimate the effect of differential cuticle organization on uni-axial membrane and on transverse-flexural Young's moduli of the cuticle in the rostral apex and head capsule using CLPT [32, 33]. The effective elastic constants of the cuticle regions of *Curculio longinasus* – estimated previously [1] – are used to construct constitutive equations for the entire cuticle of that species. The cuticle of the head capsule is estimated to have membrane and flexural moduli of $E_m = 4.77 \text{ GPa}$ and $E_f = 6.04 \text{ GPa}$, respectively. In the rostral apex these

values are reduced by approximately 72% and 60%, respectively ($E_m = 1.36 \text{ GPa}$; $E_f = 2.44 \text{ GPa}$). Two hypothetical cuticle lay-ups are also modeled to individually assess the contributions of either modified layer thickness or stacking angle sequence to the cuticle's flexibility. The effective moduli of a configuration with the angle stacking sequence of an otherwise typical cuticle (i.e., in the head capsule) that shows layer thicknesses of the rostral apex are calculated as $E_m = 3.73 \text{ GPa}$, $E_f = 4.31 \text{ GPa}$; representing 22% and 29% decreases from unmodified cuticle, respectively. Similarly, a hypothetical cuticle with the layer thicknesses of ordinary cuticle yet possessing the angle stacking sequence of the rostral apex (i.e., $\pm 45^\circ$ angle-ply in the endocuticle) has effective elastic moduli of $E_m = 3.77 \text{ GPa}$, $E_f = 5.76 \text{ GPa}$; representing 21% and 4.7% decreases from unmodified cuticle, respectively. Each of the cuticle modifications noted in the rostral apex individually decrease the elastic moduli of the cuticle. However, they appear to have a synergistic combined effect on cuticle elasticity, rather than a simple additive effect. This result suggests that both modifications are necessary in order for the snout to function properly in the living individual – where the combined effect allows the rostrum to bend until completely straight without fracture.

II. FORCE-CONTROLLED LOADING TO FRACTURE

To better characterize the failure behavior of the female rostrum, we performed tensile testing on the snouts of

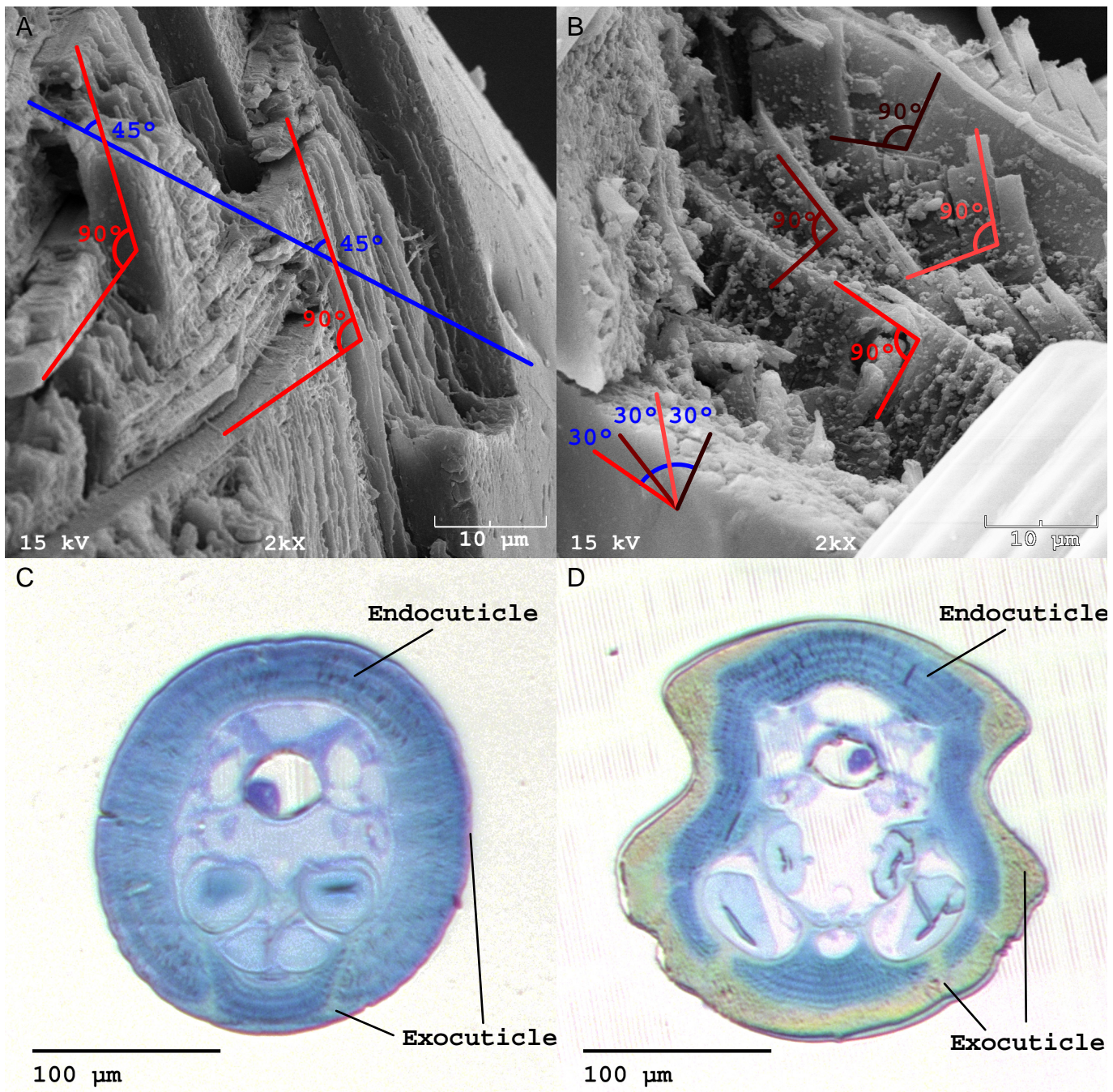


FIG. 3. Composite profiles of rostral *Curculio* cuticle. **a**, Scanning electron micrograph of fractured specimen of *Curculio humeralis* (Casey, 1897), showing that cuticle of rostral apex is organized as $\pm 45^\circ$ angle-ply laminate. **b**, Scanning electron micrograph of fractured specimen of *Curculio caryaee* (Horn, 1873), showing that cuticle of rostral base and head capsule has approximately 30° stacking angle between each pair of pseudo-orthogonal plies. **c–d**, Semi-thin sections of cuticle from specimen of *Curculio humeralis*, stained with toluidine-blue-borax; demonstrating: **(c)** that exocuticle of rostral apex is reduced to thin shell close to $5 \mu\text{m}$ thick, with endocuticle thickened to maintain a constant laminate thickness; and, **(d)** that exocuticle of head capsule and base of snout occupies nearly half of through-thickness of cuticle.

167 six *Curculio* species that representing a mixture of closely 171 uniaxial loading to fracture at a constant stress rate of
 168 and distantly related taxa [34–37]. Each specimen was 172 $1.0 \text{ gf} \cdot \text{s}^{-1}$. In general, the specimens exhibited a non-
 169 first immersed in di-H₂O for 24 hours to simulate the 173 linear viscoelastic response curve characterized by a sharp
 170 living tissue (see [38]), then subjected to force-controlled, 174 increase in stress at higher strains, terminating in brittle

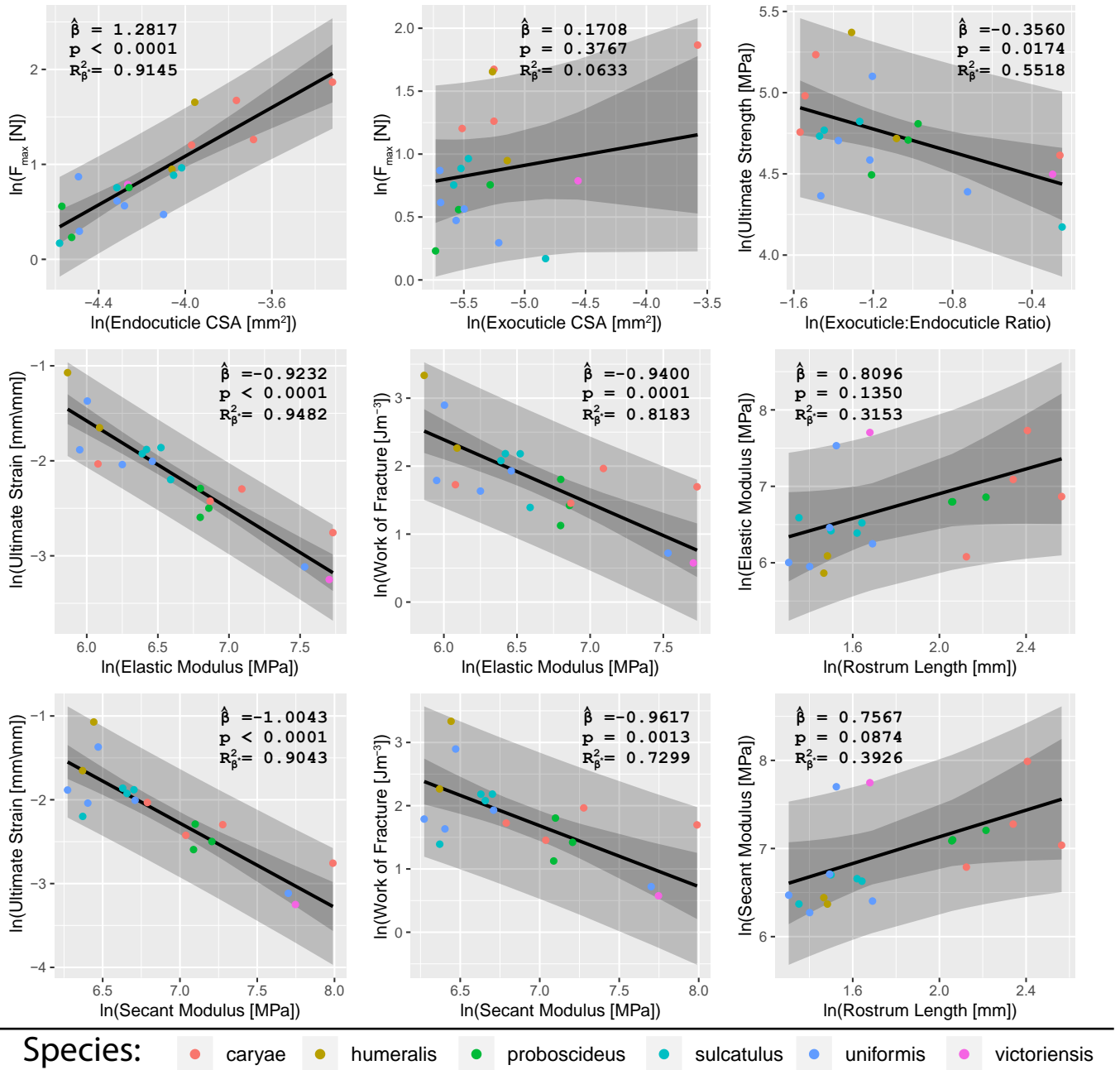


FIG. 4. Tensile properties of the female *Curculio* rostrum. Each plot shows relationship between two variables as predicted by phylogenetic linear mixed-effect model; with species as random effect and variance-covariance matrix generated from Brownian motion over preferred phylogeny of [35]. Gray regions represent the prediction interval and bootstrapped 95% confidence interval of model. The estimated fixed effect $\hat{\beta}$ is given, along with p-value of t-test assessing whether $\hat{\beta}$ is significantly different from zero. Generalized marginal R_{β}^2 for assessing fixed effects is also reported. In general, increased endocuticle thickness is associated with greater tensile strength, and stiffness is inversely correlated with toughness.

175 fracture [39]. We suggest that strain hardening occurs
176 as the longitudinal axis of the macrofibers becomes more
177 closely aligned to the cylindrical axis of the rostrum,
178 thereby resisting tension more directly with increasing
179 strain [40].

180 We also examined the correspondence between com-
181 posite structure and mechanical behavior of the snout

182 in an evolutionary, comparative context. Phylogenetic
183 linear mixed effects models (PGLM, Fig. 4) were used
184 to account for phylogenetic non-independence in residual
185 variance, with species membership included as a random
186 effect [41, 42]. The resulting models show that the max-
187 imum force sustained at the site of failure is strongly
188 correlated with the cross-sectional area of the endocu-

ticle ($\hat{\beta} = 1.28$, $p < 0.0001$), and not the exocuticle ($\hat{\beta} = 0.17$, $p = 0.38$), at that site. There is thus a negative correlation between ultimate tensile strength of the specimen and the cross-sectional exocuticle-to-endocuticle area ratio at the fracture site ($\hat{\beta} = -0.36$, $p = 0.017$). Although CLPT predicts a positive association between the proportion of exocuticle and stiffness of a generalized cuticle, we found no evidence of correspondence between the cross-sectional properties of the fracture site and the overall performance of the rostrum. This result is not too surprising however; because the cross-sectional areas of the cuticle regions vary across the length of the head along an anterior-posterior gradient, it is not possible to correlate measurements from the fracture surface to properties of the entire rostrum.

Instead, we found that the uniaxial elastic modulus (low strain: E_{low}) and secant modulus at failure (E_{sec}) were inversely correlated with ultimate strain and work of fracture (see Fig. 4). This implies that stiffer specimens – and by extension, stiffer cuticle profiles – are generally more brittle. We also observed a moderate, but not statistically significant, stiffening size-effect with respect to rostral length. This runs contrary to our expectation that a longer, more strongly curved rostrum would require increased flexibility to avoid fracture during oviposition [36, 37]. It is possible that longer rostra also have a longer transition gradient from basal to apical profile; thereby reinforcing the junction between the rostrum and head capsule against buckling. Young's modulus of the rostrum would be comparatively higher in such species, due to the higher volume fraction of exocuticle. We therefore posit that the gross elastic performance of the cuticle is consistent across the weevil genus *Curculio*. A single mechanism – i.e., the modified composite profile – likely confers increased flexibility and tensile strength to the rostral apex across all *Curculio* species. In addition, the endocuticle demonstrably contributes more to rostral tensile strength than the exocuticle; likely because of its organization into large bundles of aligned, anisotropic fibers, and amounting a trade-off between rigidity and toughness. Consequently, the altered composite profile of the cuticle in the rostral apex makes the rostrum simultaneously more flexible and fracture-resistant.

III. LOAD CYCLING OF THE PECAN WEEVIL

To confirm that repeated, prescribed straightening of the rostrum does not result in damage to the cuticle, we performed displacement-controlled fatigue testing on a typical female specimen of the pecan weevil *Curculio caryae* (Horn, 1873) – a species that exhibits extreme (80–90°, Fig. 5) rostral curvature [16, 21]. The specimen was aligned so that uniaxial tension would induce elongation of the distal portion of the rostrum with minimal off-axis deflection of the uncurved section. The strain per cycle was fixed at an amplitude sufficient to completely elongate the rostrum and generate a tensile load

of 1.0 N in the straightened configuration (ca. 20% ultimate strength), at a frequency of 0.33 Hz. The test was terminated after a period of two weeks – i.e., ca. 400,000 cycles – when the stress amplitude appeared to reach an asymptotic minimum. The rostrum behaved viscoelastically, indicated by hysteresis in the stress-strain relationship during each cycle. Strain amplitude decreased logarithmically with cycle number, and the specimen appeared to have been deformed plastically and permanently during the test. However, after cleaning the specimen in a 24-hour wash with ethanol and water, the rostrum had returned to its original shape (Fig. 5).

While we cannot fully determine the cause for rostrum stress relaxation *after* testing, we speculate that it arose from the general mechanism associated with cuticle viscoelasticity. The endocuticle is made of aligned α -chitin nanofibrils whose crystalline structure is enforced by hydrogen bonds between individual chitin chains and through the protein matrix along their length. Macroscopic viscoelastic behavior results from slippage between these chains in response to shearing between the chitin molecules [2, 43, 44]. Repeated strain may have caused such slippage in the endocuticle of the rostral apex during the fatigue test. Without sufficient time for the material to completely relax after deformation, the rostrum would slowly accumulate strain and deform viscoelastically [40]. After immersion in ethanol and water, however, the cuticle would be sufficiently plasticized to allow the rostrum to return to its original configuration, thus dissipating the accumulated strain.

The specimen did not show any evidence of fractures, micro-tears, or shear cusps anywhere in the surface of the exocuticle. Moreover, the tensile strength of the tested specimen's rostrum was consistent with that of other species members ($F_{max} = 5.02$ N). Surprisingly, the specimen remained undamaged by the testing. We therefore conclude that under normal life conditions, repeated bending of the rostrum does not exceed the yield strength of the cuticle.

IV. FRACTOGRAPHY OF *CURCULIO* TEST SPECIMENS

In light of the complex failure modes evident in the fractured specimens, it was not always possible to identify void nucleation and crack initiation sites. We observed several patterns characteristic of both the micro-scale behavior of the cuticle and the meso-scale behavior of the rostrum during uniaxial tensile failure (Fig. 6). These patterns are described below.

In transverse view, the exocuticle consistently presented a nearly continuous fracture surface. This is characteristic of comparatively brittle failure – presumably due to the relatively homogeneous arrangement of α -chitin laminae in the Bouligand structure [25, 26]. The exocuticle typically appeared to fracture at lower strains than the endocuticle, with shear-cusp formation evident both

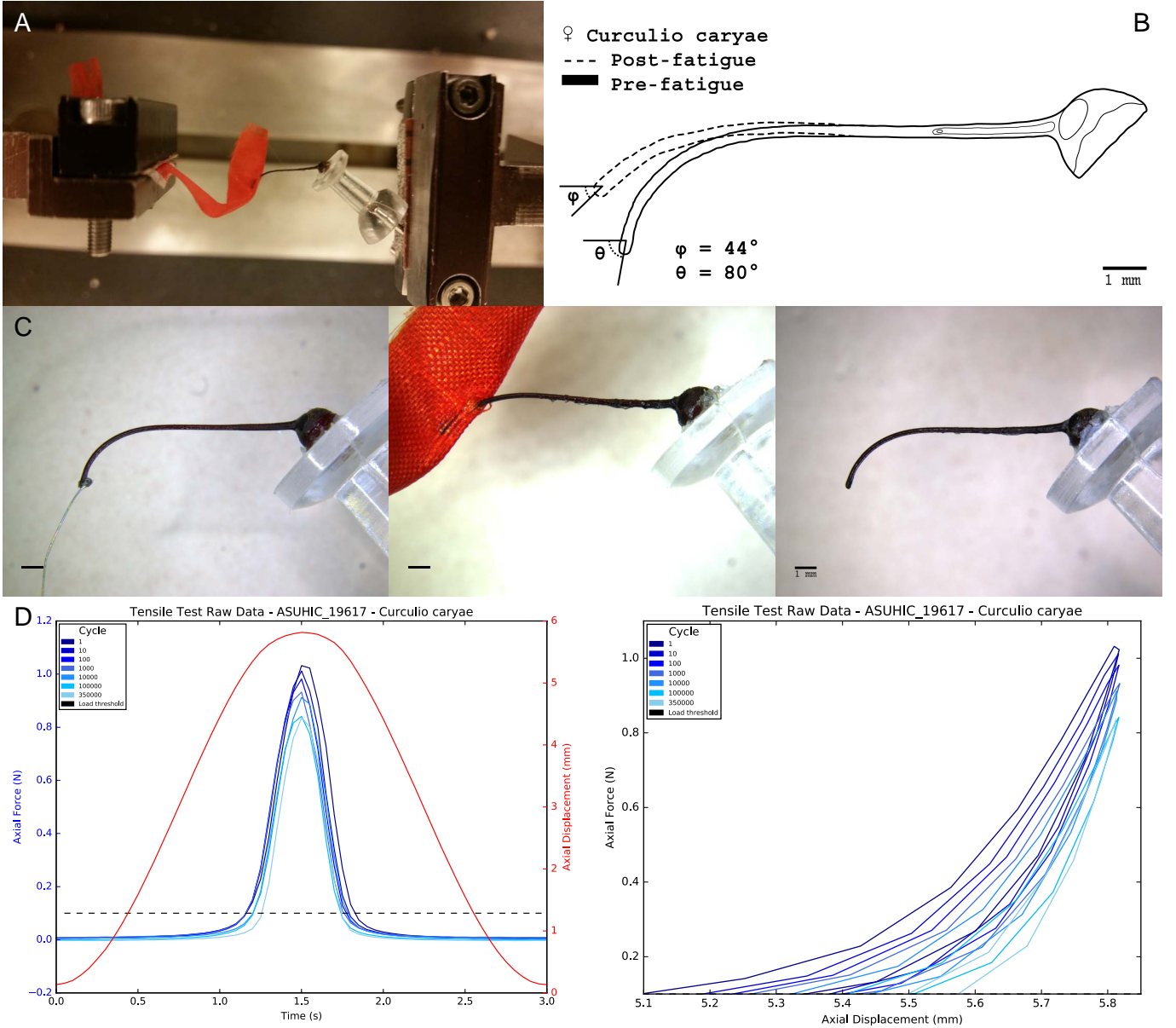


FIG. 5. Fatigue testing of a female *Curculio caryae* rostrum. **a**, Set-up of fatigue testing, with female's head capsule fixed to pedestal and rostrum attached to strip of rip-stop nylon fabric using cyanoacrylate adhesive. Specimen was loaded in tension, as opposed to compression, therefore isolating effect of tension on fatigue behavior of rostrum. **b**, Overlay of pre- and post-fatigue states of head, showing clear (short-term) effect from repeated prescribed strain. **c**, Three-photograph sequence of pre- and post-fatigue states of the rostrum; with left and central panels showing conditions immediately prior to and after testing, respectively, whereas right panel shows head having returned to its original shape after 24 hours off soaking in a water/ethanol mixture. Hence immediate post-fatigue shape is not permanent. **d**, Raw force data (left) and displacement data (right) plots for fatigue test. Displacement data plot shows clear viscoelastic behavior, indicated by hysteresis in stress-strain response of specimen, and exhibits logarithmic decrease stress amplitude over time.

299 at the fracture surface and across exocuticle adjacent 306 the endocuticle by cross-linking fibers (see [5, 23]), exocu-
300 to the plane of fracture [45]. Conversely, the endocuti- 307 ticular shear-cusp formation in uniaxial tension suggests
301 cle exhibited severe delamination, off-axis ply-splitting, 308 extension-shear coupling within individual endocuticle
302 and fiber-pulling away from the fracture surface. This 309 laminae; and further implies that ply-splitting occurred
303 is indicative of the relatively high toughness of the uni- 310 via mode II fracture between macrofibers at high strain
304 directional α -chitin organization within the macrofibers 311 [32, 33]. We hypothesize that intra-laminar extension-
305 [4, 5]. Because the exocuticle of weevils is anchored to 312 shear coupling also yielded off-axis, in-plane resultant

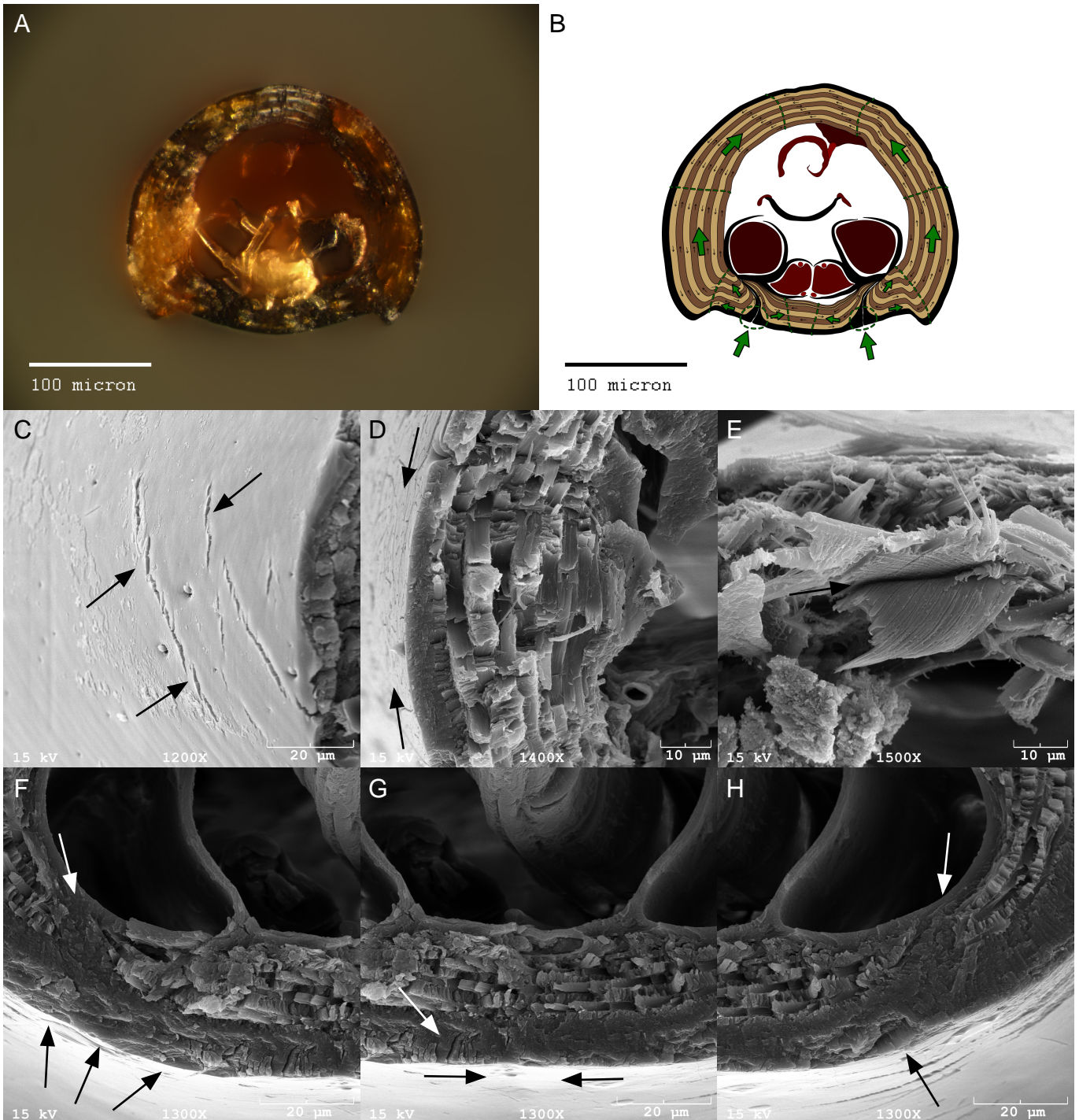


FIG. 6. Fractography of female *Curculio* rostrum. **a**, Light micrograph showing the fracture surface of tensile tested *Curculio caryae* rostrum, displaying typical failure mode; illustrated in **(b)**: Small, black arrows indicate the winding direction of macrofiber lamina; green arrows and dotted lines indicate the direction of crack. Scanning electron micrographs highlight: **(c)** shear cusp formation; **(d)** tensile failure and off-axis macrofiber fiber-pulling; **(e)** interlaminar delamination; **(f-h)** crack formation near invaginated exocuticle; and **(g)** ventral crack-front coalescence and shear cusp formation.

313 forces as a function of lamina orientation angle. Mode III 317 would ultimately occur via mixed-mode I/II – i.e., trans-
 314 shearing then occurred between laminae with opposing 318 verse tension/intra-laminar shear – fracture, due to an
 315 in-plane resultant forces, causing the observed inter-ply 319 increase in applied stress caused by ply-splitting in adj-
 316 delamination. Tensile failure of the macrofiber laminae 320 cent laminae [45].

At the meso-scale, most specimens fractured along a single plane across and between the occipital sulci, which are cuticular invaginations that traverse the entire length of the rostrum [13, 17]. These sulci increase the volume fraction of exocuticle in the ventral part of the snout. They contain large interfaces ideal for void nucleation

(Fig. 6). The exocuticle of the occipital sulci usually displayed shear cusps oriented outward from the center of the invagination, and continuing dorsolaterally and ventromedially. Ventrally, the cusps converged toward a prominent scarp where the crack fronts joined. This scarp was often obscured by delaminated endocuticular macrofibers in specimens with large cross-sectional areas of endocuticle,

The first layer of endocuticle usually fractured along the same plane as the exocuticle. Ventrally, the endocuticle laminae typically converged toward a scarp-like region characterized by severe delamination and numerous debonded macrofibers. Moreover, macrofibers aligned with the direction of crack propagation exhibited extensive ply-splitting with intermittent transverse shearing. In contrast, macrofibers oriented against the direction of crack propagation primarily displayed fracture by transverse shear along the plane of ply-splitting in adjacent laminae. Because the laminae form a cylinder, contralateral fibers in the same lamina display opposing fracture modes. The ventrolateral surfaces often exhibited extensive inter-ply delamination and fiber de-bonding in scarp-like prominences. This is likely due to a combination of tensile failure and shearing along the dorsally-radiating crack front. Dorsally, the coalescent crack fronts often caused significant de-bonding and ply-splitting, followed by broom-like tensile failure. In some specimens, the contralateral crack fronts were out of plane and coalesced via transverse shear through a large dorsal section of cuticle.

Based on these failure patterns, we hypothesize that the exocuticle-rich occipital sulci are the most likely site for the initiation of void nucleation and catastrophic failure of the integrated rostral cuticle in cross section, as illustrated in Fig. 6. Structural failure would take place as cracks propagate through the endocuticle from these sutures, and ultimately penetrating the entire thickness of the laminate [13]. Although other, more complex failure modes have been observed, we posit that in live specimens this is the most likely mechanism of tensile failure because typical bending behavior generates tension *only* along the ventral surface of the rostrum.

V. CONCLUSIONS

The rostrum of *Curculio* is characterized by a discontinuous composite profile. The cuticle is strongly differentiated in terms of relative layer thicknesses and orientation angles along an anterior-posterior gradient. These modifications are sufficient to achieve a marked reduction in the effective membrane and flexural moduli of the cuticle – 72% and 60%, respectively – in constitutive models based

on CLPT, thereby accounting for the observed flexibility of the rostral apex in live specimens. However, the reductions can only be realized with *both* modifications to the cuticle, which have a non-additive effect on cuticle elasticity. *Curculio* females require both modifications to function properly during oviposition.

Likewise, tensile and fatigue testing reveal a trade-off between stiffness and fracture resistance – measured by ultimate strain and toughness – mediated by the relative proportion of endocuticle in the laminate. The altered composite profile of the cuticle in the rostral apex makes the rostrum simultaneously more flexible and fracture resistant, permitting the structure to be flexed without exceeding the elastic limits of the cuticle.

This is to our knowledge the first time in arthropods that the composite profile of the cuticle has been related to a gradient in elasticity and tensile performance across a cuticular structure. Because these associations are independent of species membership, we posit that the behavior of the cuticle is consistent across the genus. Rostral flexibility is achieved exclusively in all *Curculio* species through a modified cuticle lay-up. This inference raises the intriguing possibility that a single ancestral shift in cuticle organization at the rostral apex – yielding higher flexibility and tensile strength – enabled the evolutionary “exploration” of a large morphospace region, promoting the high species-level diversity of this lineage.

Based on fractographic analysis of the test specimens, we infer that the exocuticle exhibits brittle fracture at a comparatively low strain, due to shearing between the endocuticle macrofibers to which it is anchored. These macrofibers fail at higher strain, mediated by mixed-mode shearing and tensile fracture within and between laminae. This outcome is consistent with behavior shown in previous studies, as well as theoretical consideration of cuticle microstructure in CLPT. The latter predicts extension shear-coupling ($A_{16}, A_{26} \neq 0$) for individual off-axis macrofiber laminae [32, 33].

Our results imply that fracture initiation occurs in the comparatively brittle exocuticle. The reduction in exocuticle thickness in the rostral apex might serve to mitigate crack formation in rostral bending. Based on this pattern of fracture behavior, we identified the exocuticle-rich occipital suture as a common point of void nucleation and crack initiation. From an evolutionary perspective, these findings reveal an unexpected morphological source of constraint on rostral flexibility, raising the intriguing possibility that this system evolved primarily via negative selection of fracture, rather than positive selection of flexibility. In particular, the cuticle is invaginated in precisely the portion of the snout that experiences the

greatest degree of tension during antero-dorsal flexion. The doubly-thick exocuticle in the invagination thus creates an unavoidable, brittle weak-point in an otherwise endocuticle-dominated rostral apex. This constraint – in conjunction with the minimization of exocuticle thickness in the rostral apex and the increased toughness derived from a thickened endocuticle – lead us to consider that

434 avoidance of catastrophic structural failure has been a
 435 driving selective pressure in the evolution of the female
 436 *Curculio* rostrum.

437 VI. METHODS

438 Methods, including statements of data availability and
 439 any associated accession codes and references, are avail-

441 REFERENCES

- 442 [1] Jansen, M. A., Singh, S. S., Chawla, N., & Franz, N.
 443 M. A multilayer micromechanical model of the cuticle of
 444 *Curculio longinasus* Chittenden, 1927 (Coleoptera: Cur-
 445 culionidae). *J. Struct. Biol.* **195**: 2, 139–158, (2016).
- 446 [2] Vincent, J. F. V. & Wegst, U. G. K. Design and mech-
 447 anical properties of insect cuticle. *Arthropod Struct. Dev.*
 448 **33**:3, 187–199, (2004).
- 449 [3] Hepburn, H. R. & Ball, A. On the structure and mechani-
 450 cal properties of beetle shells. *J. Mater. Sci.* **8**:5, 618–623,
 451 (1973).
- 452 [4] van de Kamp, T. & Greven, H. On the architecture of
 453 beetle elytra. *Entomol. Heute* **22**, 191–204, (2010).
- 454 [5] van de Kamp, T., Riedel, A. & Greven, H. Micromorphol-
 455 ogy of the elytral cuticle of beetles, with an emphasis on
 456 weevils (Coleoptera : Curculionoidea) *Arthropod Struct.*
 457 *Dev.* **45**:1, 14–22, (2016).
- 458 [6] Neville, A. C., Parry, D. A. & Woodhead-Galloway, J.
 459 The chitin crystallite in arthropod cuticle. *J. Cell Sci.*
 460 **21**:1, 73–82, (1976).
- 461 [7] Amini, S., Tadayon, M., Idapalapati, S., and Miserez, A.
 462 The role of quasi-plasticity in the extreme contact damage
 463 tolerance of the stomatopod dactyl club *Nat. Mater.* **14**:9,
 464 943–950, (2015).
- 465 [8] McCullough, E. L., Tobalske, B. W., and Emlen, D. J.
 466 Structural adaptations to diverse fighting styles in sexually
 467 selected weapons *Proc. Natl. Acad. Sci. USA* **111**:40,
 468 14484–14488, (2014).
- 469 [9] McCullough, E. L. Mechanical limits to maximum weapon
 470 size in a giant rhinoceros beetle *Proc. R. Soc. B* **281**,
 471 20140696, (2014).
- 472 [10] Dirks, J., Parle, E., and Taylor, D. Fatigue of insect
 473 cuticle *J. Exp. Biol.* **216**:10, 1924–1927, (2013).
- 474 [11] Dirks, J. and Taylor, D. Fracture toughness of locust
 475 cuticle *J. Exp. Biol.* **215**:9, 1502–1508, (2012).
- 476 [12] *International Code of Zoological Nomenclature* Fourth
 477 Edition. (The International Trust for Zoological Nomen-
 478 clature, London, 1999).
- 479 [13] Davis, S. R. *Morphology, phylogeny, and evolutionary*
 480 *development in the weevils (Insecta: Coleoptera: Cur-*
481 culionoidea) (Ph.D. thesis, University of Kansas, 2014).
- 482 [14] Singh, S. S., Jansen, M. A., Franz, N. M., and Chawla,
 483 N. Microstructure and nanoindentation of the rostrum of
 484 *Curculio longinasus* Chittenden, 1927 (Coleoptera: Cur-
 485 culionidae) *Mater. Charact.* **118**, 206–211, (2016).
- 486 [15] Toju, H. and Sota, T. Imbalance of predator and prey
 487 armament: geographic clines in phenotypic interface and
 488 natural selection *Am. Nat.* **167**:1, 105–117, (2006).
- 489 [16] Gibson, L. P. Monograph of the genus *Curculio* in the
 490 New World (Coleoptera: Curculionidae). Part I. United
 491 States and Canada *Misc. Publ. Entomol. Soc. Am.* **6**,
 492 239–285, (1969).
- 493 [17] Dennell, R. The structure and function of the mouth-parts,
 494 rostrum and fore-gut of the weevil *Calandra granaria* L.
 495 *Phil. Trans. R. Soc. Lond. B* **231**:581, 247–291, (1942).
- 496 [18] Morimoto, K. and Kojima, H. Morphologic characters of
 497 the weevil head and phylogenetic implications (Coleoptera,
 498 Curculionoidea) *Esakia* **43**, 133–169, (2003).
- 499 [19] Ting, P. C. Feeding mechanisms of weevils, their function,
 500 and relationship to classification *Mon. Bull. Dep. Agric.*
 501 *State Calif.* **22**, 161–165, (1933).
- 502 [20] Ting, P. C. The mouth parts of the coleopterous group
 503 Rhynchophora *Microentomology* **1**, 93–114, (1936).
- 504 [21] Aguirre Uribe, L. A. *Biology of the immature stages of*
 505 *the pecan weevil Curculio caryae (Horn) and oviposition*
 506 *habits of the adult weevil* (Ph.D. thesis, Texas A & M
 507 University, 1978).
- 508 [22] Moffett, M. Life in a nutshell *Natl. Geogr. Mag.* **176**,
 509 783–784, (1989).
- 510 [23] Longhai, L. et al. Microstructure and mechanical proper-
 511 ties of rostrum in *Cyrtotrachelus longimanus* (Coleoptera:
 512 Curculionidae) *Anim. Cells Syst.* **21**:3, 199–206, (2017).
- 513 [24] Matsumura, Y., Kovalev, A. E., and Gorb, S. N. Pen-
 514 tration mechanics of a beetle intromittent organ with
 515 bending stiffness gradient and a soft tip, *Sci. Adv.* **3**:12,
 516 eaao5469, (2017).
- 517 [25] Nikolov, S. et al. Robustness and optimal use of design
 518 principles of arthropod exoskeletons studied by ab initio
 519 based multiscale simulations. *J. Mech. Behav. Biomed.*
 520 *Mater.* **4**:2, 129–145, (2011).
- 521 [26] Nikolov, S. et al. Revealing the design principles of high-
 522 performance biological composites using Ab initio and
 523 multiscale simulations: The example of lobster cuticle.
 524 *Adv. Mater.* **22**:4, 519–526, (2010).
- 525 [27] Blackwell, J. and Weih, M. Structure of chitin-protein
 526 complexes: ovipositor of the ichneumon fly *Megarhyssa*.
 527 *J. Mol. Biol.* **137**:1, 49–60, (1980).
- 528 [28] Bouligand, Y. Twisted fibrous arrangements in biological
 529 materials and cholesteric mesophases. *Tissue Cell* **4**:2,
 530 189–217, (1972).
- 531 [29] Vincent, J. F. V. *Structural biomaterials* (Halsted Press,
 532 New York, 1982).
- 533 [30] Cheng, L., Wang, L., & Karlsson, A. M. Mechanics-based
 534 analysis of selected features of the exoskeletal microstruc-
 535 ture of *Popillia japonica*. *Mater. Res.* **24**:11, 3253–3267,
 536 (2009).
- 537 [31] Leopold, R. A., Newman, S. M., and Helgeson, G. A
 538 comparison of cuticle deposition during the pre-and poste-

- 539 closion stages of the adult weevil, *Anthonomus grandis* 597
 540 BOHEMAN (Coleoptera: Curculionidae) *Int. J. Insect*
 541 *Morphol. and Embryol.*, **21:1**, 37–62, (1992).
- 542 [32] Reddy, J. N. *Mechanics of laminated composite plates* 598
 543 and shells: theory and analysis (CRC Press, Philadelphia, 599
 544 2004).
- 545 [33] Jones, R. M. *Mechanics of composite materials* (CRC 600
 546 press, Philadelphia, 2014).
- 547 [34] Hughes, J. and Vogler, A. P. The phylogeny of acorn 601
 548 weevils (genus *Curculio*) from mitochondrial and nuclear 602
 549 DNA sequences: the problem of incomplete data *Mol. 603*
Phylogenetic Evol. **32:2**, 601–615, (2004).
- 550 [35] Bonal, R. et al. Diversity in insect seed parasite guilds at 604
 552 large geographical scale: the roles of host specificity and 606
 553 spatial distance *J. Biogeogr.* **43:8**, 1620–1630, (2016).
- 554 [36] Hughes, J. and Vogler, A. P. Ecomorphological adaptation 607
 555 of acorn weevils to their oviposition site *Evolution* **58:9**, 608
 556 1971–1983, (2004).
- 557 [37] Bonal, R., Espelta, J. M., and Vogler, A. P. Complex 609
 558 selection on life-history traits and the maintenance of 610
 559 variation in exaggerated rostrum length in acorn weevils 611
Oecologia **167:4**, 1053–1061, (2011).
- 560 [38] Klocke, D. & Schmitz, H. Water as a major modulator of 612
 562 the mechanical properties of insect cuticle. *Acta Biomater.* 7, 2935–2942 (2011).
- 564 [39] Mihai, L. A. and Goriely, A. How to characterize a nonlin- 613
 565 ear elastic material? A review on nonlinear constitutive 614
 566 parameters in isotropic finite elasticity *Phil. Trans. R. 615*
Soc. Lond. A **473:2207**, 20170607, (2017).
- 568 [40] Münster, S. et al. Strain history dependence of the nonlin- 616
 569 ear stress response of fibrin and collagen networks *Proc. 617*
Natl. Acad. Sci. USA **110:30**, 12197–12202, (2013).
- 571 [41] Felsenstein, J. Phylogenies and the comparative method 618
Am. Nat. **125:1**, 1–15, (1985).
- 573 [42] Revell, L. J. Phylogenetic signal and linear regression on 619
 574 species data *Methods Ecol. Evol.* **1:4**, 319–329, (2010).
- 575 [43] Beament, J. W. L., Treherne, J. E., and Wigglesworth, 620
 576 V. B. *Advances in insect physiology* Volume 4 (Academic 621
 577 Press Inc., London, 1967).
- 578 [44] Sun, J. Y. et al. Differential constitutive equation of elytra 622
 579 cuticle by nanoindentation *Adv. Mater. Res.*, **343**, 1133– 623
 580 1139, (2012).
- 581 [45] Greenhalgh, E. *Failure analysis and fractography of poly- 624*
 582 *mer composites* (CRC Press, Boca Raton, 2009).

AUTHOR CONTRIBUTIONS

598 M.A.J. conducted sectioning and staining, microscopy 599 and imaging, tensile and fatigue testing, statistical anal- 600 ysis, and participated in manuscript preparation. J.W. 601 conducted tensile and fatigue testing and participated 602 in manuscript preparation. N.C. facilitated microscopy, 603 tensile and fatigue testing, and participated in manuscript 604 preparation. N.M.F. facilitated specimen acquisition and 605 imaging and participated in manuscript preparation.

ADDITIONAL INFORMATION

607 Supplementary information is available in the online ver- 608 sion of the paper. Reprints and permissions information 609 is available online at www.nature.com/reprints. Corre- 610 spondence and requests for materials should be addressed 611 to M.A.J.

COMPETING FINANCIAL INTERESTS

613 The authors declare no competing financial interests.

ACKNOWLEDGMENTS

584 The authors are grateful to Robert Anderson (CMNC),
 585 Lourdes Chamorro (USNM), and Charlie O'Brien
 586 (CWOB) for their assistance and provision of *Curculio*
 587 specimens used in this study. The authors thank Salvatore
 588 Anzaldo, Andrew Johnston, Brian Reilly, Sangmi
 589 Lee, and other Arizona State University Hasbrouck In-
 590 sect Collection (ASUHIC) members for their assistance in
 591 procuring, treating, and maintaining specimen loans upon
 592 entry into the ASUHIC. The authors would also like to
 593 thank David Lowry (ASU CLAS Bioimaging Center) for
 594 his training and assistance with resin embedding, scanning
 595 electron microscopy, and microtomography; and Salvatore
 596 Anzaldo for his assistance with histological staining.

614

METHODS

615

Specimen acquisition and taxon sampling

616 Specimens for use in tensile and fatigue testing came
 617 from the Hasbrouck Insect Collection at Arizona State
 618 University [ASUHIC]. This set of specimens was supple-
 619 mented with material housed in the following collections,
 620 using the codens of Arnett et al. [46]:

621 CMNC: Canadian Museum of Nature Collection, Ottawa,
 622 Ontario, Canada

623 USNM: National Museum of Natural History, Washington,
 624 D.C., USA

625 Cold fracture, semi-thin sectioning, and tensile testing
 626 were conducted on randomly chosen female specimens
 627 belonging to six *Curculio* species obtainable through field
 628 work in the southwestern United States and northwest-
 629 ern Mexico. Taxon sampling was targeted to represent
 630 a mixture of disparate radiations and sister taxa with
 631 a variety of rostral morphotypes in accordance with the
 632 phylogenetic hypotheses of Hughes et al. [34, 36] and
 633 Bonal et al. [35]. The six species of *Curculio* used herein
 634 are (in alphabetical sequence): *Curculio caryae* (Horn,
 635 1873), *Curculio humeralis* (Casey, 1897), *Curculio pro-*
boscideus Fabricius, 1775, *Curculio sulcatulus* (Casey,
 637 1897), *Curculio uniformis* (LeConte, 1857), and *Cur-*
culio victoriensis (Chittenden, 1904). Specimens were
 639 identified to taxonomic (species) concepts using [16] and
 640 other resources.

641

Histological sectioning

642 To illustrate the relative proportions of the cuticle re-
 643 gions in cross-section, serial semi-thin sectioning was con-
 644 ducted on exemplary female specimens of *Curculio humer-*
alis and *Curculio longinasus* Chittenden, 1927. Live spec-
 646 imens of both species were collected into 95% ethanol
 647 for preservation. A female specimen was selected; and
 648 the rostrum was separated from the head capsule with a
 649 fine-edged razor blade. The apical 1/4th of the rostrum
 650 was also removed and then discarded. The remaining
 651 portion of the rostrum and the head capsule were then
 652 embedded in EMbed812, as follows.

653 The cuticle was first immersed in acetone for 24 hours,
 654 and then transferred to a 2:1 mixture of acetone to epoxy
 655 resin. Samples remained at 21°C for 12 hours on a shaker
 656 table to prevent hardening. They were then transferred
 657 into a 1:1 mixture of acetone to resin, followed by a
 658 1:2 mixture (each for 12 hours and at 21°C on a shaker
 659 table), before finally being placed into a silicone mold
 660 with pure resin. The mold was placed into an oven heated
 661 to 38°C, and the resin was allowed to cure for 24 hours.
 662 The resulting blocks were machined to prepare the apical
 663 surface of each sample for microtomy.

664 A Leica Ultracut R Microtome and diamond knife were
 665 used to expose a cross-section (transverse plane) of the
 666 apical and basal portions of the rostrum and to remove ex-
 667 cess material. Semi-thin sections (0.5 µm thick) were kept
 668 and stained with toluidine-blue-borax for light microscopy
 669 and imaging.

670

Cold-fracture of specimens

671 Two pinned female specimens of each *Curculio* species
 672 were selected at random and retained for cold-fracturing
 673 of the rostrum. The heads of the specimens were removed
 674 and cleaned using a 95% ethanol solution and a thin paint-
 675 brush. Any muscles protruding from the occipital foramen
 676 were removed with a fine-edged razor blade. The anten-
 677 nae were removed directly using forceps to pull the scape
 678 (basal section of antenna) from the antennal insertion.
 679 Cleaned specimens were stored at -80°C for 24 hours,
 680 then fractured using forceps over a chilled aluminum block.
 681 To fracture each specimen, the head capsule and rostrum
 682 were each gripped firmly in a pair of forceps. The forceps
 683 were then sharply rotated to fracture the base of the snout
 684 via dorsal flexion. The rostrum was fractured a second
 685 time, after separation from the head capsule, using the
 686 same procedure. The segmented specimens were then
 687 placed into individual glass vials to protect the fracture
 688 surfaces from contamination prior to microscopy.

689

Tensile and fatigue testing

690 *Force-controlled loading to failure.* Five female speci-
 691 mens of each *Curculio* species were randomly allocated
 692 for use in tensile testing. The head of each specimen was
 693 removed, cleaned, and prepared as described above in the
 694 cold-fracture protocol. To avoid destroying the delicate,
 695 brittle specimens when gripping the ends of each head, a
 696 method was devised to create solid handles that could be
 697 clamped tightly into grips without risk of damage to the
 698 cuticle.

699 For each head, four 1 cm² strips of gaffer tape were
 700 cut; these were used as gripping and mounting points
 701 for the specimen. A strip of tape would be laid flat,
 702 with a large drop of cyanoacrylate glue placed upon the
 703 upturned surface. The curved portion of the snout was
 704 then placed into the drop, such that the straight portion
 705 of the rostrum was aligned perpendicular to the edge
 706 of the strip. Hardening of the cyanoacrylate effectively
 707 embedded the curved portion of the snout in a solid
 708 mass, isolating a straight section of the snout – from the
 709 base to a point distad of the apex of the scrobe – for
 710 testing. A second strip of tape was fixed over this mass
 711 with an additional layer of cyanoacrylate to provide a
 712 dorsal gripping surface for the mass. A small mark was
 713 made to indicate the extent of the head inside the mass.
 714 This embedding procedure was repeated for the head

715 capsule, resulting in a finished specimen with anterior 770
 716 and posterior handles for testing.

717 Prior to testing, each specimen was placed in de-ionized 771
 718 water for 24 hours to allow full saturation of the cuticle, 772
 719 simulating the condition of live tissue [38]. Once removed 773
 720 for testing, the specimen was gripped using the cyanoacry- 774
 721 late handles at the marked locations immediately beyond 775
 722 the anterior margin of the rostrum and the posterior mar- 776
 723 gin of the head capsule. The exposed section of the snout 777
 724 was coated in petroleum jelly using a cotton swab to 778
 725 prevent loss of moisture and stiffening of the specimen 779
 726 during the test. Specimens were loaded in a Tryton 250 780
 727 Microforce Testing System equipped with a 5N load cell 781
 728 and mechanical clamp grip. All specimens were subjected 782
 729 to force-controlled uniaxial tension at a rate of $1.0 \text{ gf} \cdot \text{s}^{-1}$ 783
 730 until failure, with a sampling interval of 0.1 s. Engineer- 784
 731 ing stresses ($\sigma_0 = F/A_0$) and strains ($\epsilon_0 = \Delta l/l_0$) were 785
 732 reported only for specimens that did not fracture due to 786
 733 strain accumulation at the interface between the rostrum 787
 734 and the cyanoacrylate handles.

735 *Displacement-controlled cyclic loading.* To confirm 788
 736 that repeated, complete extension of a strongly curved 789
 737 rostrum would not result in fracture of the cuticle, a 790
 738 representative female specimen of *Curculio caryae* was 791
 739 allocated for fatigue testing. The head capsule of the 792
 740 specimen was fixed to a push-pin using cyanoacrylate 793
 741 glue. This served as a pedestal and gripping location 794
 742 for the posterior portion of the specimen. The apex of 795
 743 the rostrum was fixed to a strip of ripstop nylon fabric 796
 744 equal in length to the head, using cyanoacrylate glue. As 797
 745 with tensile testing, the specimen was placed in de-ionized 798
 746 water for 24 hours, then coated in petroleum jelly using 799
 747 a cotton swab immediately prior to load cycling.

748 The end of the fabric was gripped and used to elongate 780
 749 the rostrum in tension by pulling on the fabric, thus 781
 750 isolating the effect of tension on the fatigue life of the 782
 751 rostral cuticle. In this way, the rostrum would return to 783
 752 its original configuration in a spring-like manner, as in 784
 753 living specimens, rather than being forced to return to the 785
 754 initial position. The rostrum was aligned such that complete 786
 755 elongation of the curved section would take place in 787
 756 tension, with minimal off-axis deflection of the un-curved 788
 757 section. The specimen was subjected to displacement- 789
 758 controlled loading sufficient to fully extend the rostrum 790
 759 and generate a load stress of 1 N, or approximately 20% of 791
 760 the tensile strength of the species average. Load cycling 792
 761 took place at a rate of 0.33Hz, and was continued for 14 793
 762 days – i.e., 400,000 cycles – until the tensile stress in the 794
 763 sample approached an asymptotic minimum.

764 Once the test was concluded, the specimen was placed in 806
 765 a 50% ethanol solution for 24 hours to clean the petroleum 807
 766 jelly from the rostrum. The specimen was examined for 808
 767 surface fractures and micro-tears, then subjected to tensile 809
 768 testing via the same protocol as the other specimens to 810
 769 assess whether the cuticle had begun to fatigue.

Specimen imaging and microscopy

771 The fracture surfaces of cold-fractured specimens were 772
 773 examined using scanning electron microscopy to charac- 774
 775 terize the composite profile and microstructure of the 776
 777 rostrum. Fracture behavior of tensile testing specimens 778
 779 was assessed using both light microscopy and SEM to 779
 780 image the fracture surfaces of the specimens in transverse 781
 782 view. Electron microscopy was conducted using a JEOL 783
 784 JSM6300 scanning electron microscope. Light microscopy 785
 786 was conducted using a Leica M205 C stereomicroscope 787
 788 and attached computer running the software Leica Appli- 788
 789 cation Suite (LAS); as well as a Visionary Digital Passport 789
 790 II system using a Canon EOS Mark 5D II camera outfit- 790
 791 ted with interchangeable macro lenses. Specimen length, 792
 793 layer thicknesses, macrofiber orientation angles, and cross- 793
 794 sectional areas were measured in the LAS and in Adobe 794
 795 Illustrator, using pixel-wise measurements multiplied by 795
 796 a scaling factor for the image.

Constitutive modeling of the cuticle

789 *General approach.* The effective uni-axial membrane 790
 790 and transverse flexural elastic moduli of idealized cuticle 791
 791 organizations, representing both the rostral apex and head 792
 792 capsule, were estimated using Classical Laminate Plate 793
 793 Theory (CLPT). For general information on this approach 794
 794 see [32, 33]. The composite profiles of both types of cuticle 795
 795 were idealized using the layer thicknesses and stacking se- 796
 796 quences observed in *Curculio longinasus*. This particular 797
 797 species was chosen because we derived the effective elastic 798
 798 constants of the individual components of the cuticle in 799
 799 previous work [1, 14]. In addition, *Curculio longinasus* 800
 800 exhibits a profile that is typical and representative for the 801
 801 genus *Curculio*, based on examination of the six species 802
 802 used for tensile testing.

803 For *Curculio longinasus* the total thickness of the 804
 804 cuticle in the head and rostrum is roughly 50 μm , 805
 805 as in most specimens of the other examined species. 806
 806 In the head capsule, the exocuticle occupies between 807
 807 30-50% of the through-thickness of the laminate, with 808
 808 the remaining thickness nearly evenly divided between 809
 809 12 layers of endocuticle. We use the maximum (50% 810
 810 of through-thickness, or 25 μm) for the model, since 811
 811 the cuticle appears to deviate from this value only in 812
 812 regions with sulci (grooves), pores, and other scattered 813
 813 features of the surface sculpture. The macrofiber lami- 814
 814 nae of the endocuticle were assigned a stacking sequence of 815
 815 $0^\circ, 90^\circ, 30^\circ, -60^\circ, 60^\circ, -30^\circ, 90^\circ, 0^\circ, -60^\circ, 30^\circ, -30^\circ, 60^\circ;$ 816
 816 thereby representing pairs of orthogonal plies stacked at 817
 817 a constant rotation angle of 30° , in approximation of the 818
 818 living tissue.

819 In the rostral apex, the exocuticle is reduced to a thin 820
 820 shell approximately 5 μm in thickness, or 10% of the 821
 821 total cuticle thickness. The endocuticle displays a more 822
 822 complex pattern of layer thicknesses in the rostral apex 823
 823 than in the head capsule. Each of the eight outermost

⁸²⁴ layers are of nearly equal thickness to the exocuticle (5
⁸²⁵ μm), whereas the four innermost layers have a combined
⁸²⁶ thickness equal to that of the exocuticle or to a single layer
⁸²⁷ of outer endocuticle ($h_{\text{outer}} = 5 \mu\text{m}$, $h_{\text{inner}} = 1.25 \mu\text{m}$).
⁸²⁸ The stacking sequence with respect to the longitudinal
⁸²⁹ axis of the rostrum forms an antisymmetric angle-ply
⁸³⁰ laminate of $\pm 45^\circ$.

⁸³¹ To assess the individual contributions of layer thickness
⁸³² and stacking angle sequence to cuticle flexibility in the
⁸³³ rostral apex, two hypothetical cuticle lay-ups were mod-
⁸³⁴ eled – each with only one of the modifications present in
⁸³⁵ the cuticle of the rostral apex. The first of these models
⁸³⁶ has the layer thicknesses of the rostral apex, but fiber
⁸³⁷ orientations of the head capsule; whereas the second has
⁸³⁸ the fiber orientations of the rostral apex, but the layer
⁸³⁹ thicknesses of the head capsule.

⁸⁴⁰ Because these laminates are not symmetric, each has
⁸⁴¹ a bending-extension coupling matrix $[B]$ populated with
⁸⁴² non-zero terms; thus complicating the calculation of effec-
⁸⁴³ tive in-plane elastic moduli. To circumvent this difficulty
⁸⁴⁴ and enable meaningful comparisons between each lam-
⁸⁴⁵ inate, all of the lay-ups are reflected about their inner
⁸⁴⁶ surface. This effectively doubles their thickness while pro-
⁸⁴⁷ ducing a balanced, symmetric laminate with no coupling
⁸⁴⁸ between bending and extension (i.e., $[B] = 0_{3,3}$). Estima-
⁸⁴⁹ tion of in-plane elastic constants from the extension($[A]$)
⁸⁵⁰ and bending ($[D]$) matrices is described in detail below.
⁸⁵¹ The program Matlab R2018b was used to numerically
⁸⁵² evaluate the final values of the effective elastic constants
⁸⁵³ [47].

⁸⁵⁴ *Classical Laminate Plate Theory.* We begin by calcu-
⁸⁵⁵ lating the 2D reduced stiffness matrix for each part of the
⁸⁵⁶ cuticle. For orthotropic materials with the principal axes
⁸⁵⁷ parallel to the ply edges, the reduced stiffness matrix is
⁸⁵⁸ defined as follows:

$$[Q] = \begin{bmatrix} Q_{11} & Q_{12} & 0 \\ Q_{21} & Q_{22} & 0 \\ 0 & 0 & Q_{66} \end{bmatrix}, \quad (1)$$

⁸⁵⁹ where:

$$\begin{aligned} Q_{11} &= \frac{E_1}{1 - \nu_{12}\nu_{21}}, \\ Q_{12} &= \frac{E_1\nu_{21}}{1 - \nu_{12}\nu_{21}} = Q_{21}, \\ Q_{21} &= \frac{E_2\nu_{12}}{1 - \nu_{12}\nu_{21}} = Q_{12}, \\ Q_{22} &= \frac{E_2}{1 - \nu_{12}\nu_{21}}, \\ Q_{66} &= G_{12}. \end{aligned} \quad (2)$$

⁸⁶⁰ For each layer k , the reduced stiffness matrix is trans-
⁸⁶¹ formed to account for the layer orientation angle θ within
⁸⁶² the laminate coordinate system, yielding a reduced trans-
⁸⁶³ formed stiffness matrix according to:

$$[\bar{Q}] = [T]^{-1}[Q][T]^{-T}, \quad (3)$$

⁸⁶⁴ where the transformation matrix $[T]$ is defined as:

$$[T] = \begin{bmatrix} \cos^2 \theta & \sin^2 \theta & 2 \cos \theta \sin \theta \\ \sin^2 \theta & \cos^2 \theta & -2 \cos \theta \sin \theta \\ -\cos \theta \sin \theta & \cos \theta \sin \theta & \cos^2 \theta - \sin^2 \theta \end{bmatrix}. \quad (4)$$

⁸⁶⁵ Using the lay-ups specified for each type of cuticle
⁸⁶⁶ described above, we calculate the extensional stiffness
⁸⁶⁷ matrix $[A]$, bending stiffness matrix $[D]$, and bending-
⁸⁶⁸ extension coupling matrix $[B]$ for each laminate consisting
⁸⁶⁹ of n layers at a distance z from the laminate mid-plane.
⁸⁷⁰ The elements of these matrices can be identified according
⁸⁷¹ to:

$$\begin{aligned} A_{ij} &= \sum_{k=1}^n (\bar{Q}_{ij})_k (z_k - z_{k-1}), \\ B_{ij} &= \frac{1}{2} \sum_{k=1}^n (\bar{Q}_{ij})_k (z_k^2 - z_{k-1}^2), \\ D_{ij} &= \frac{1}{3} \sum_{k=1}^n (\bar{Q}_{ij})_k (z_k^3 - z_{k-1}^3). \end{aligned} \quad (5)$$

⁸⁷² These stiffness matrices respectively relate vectors of
⁸⁷³ resultant forces $\{N\}$ and bending moments $\{M\}$ to mid-
⁸⁷⁴ surface strains and curvatures $\{\epsilon^\circ\}$ and $\{\kappa\}$ in the lami-
⁸⁷⁵ nate, according to the following relationship:

$$\begin{Bmatrix} \{N\} \\ \{M\} \end{Bmatrix} = \begin{bmatrix} [A] & [B] \\ [B] & [D] \end{bmatrix} \begin{Bmatrix} \{\epsilon^\circ\} \\ \{\kappa\} \end{Bmatrix}. \quad (6)$$

⁸⁷⁶ For symmetric laminates, $[B] = 0_{3,3}$, and therefore:

$$\begin{aligned} \{N\} &= [A]\{\epsilon^\circ\}, \\ \{M\} &= [D]\{\kappa\}, \end{aligned} \quad (7)$$

⁸⁷⁷ or, in expanded form:

$$\begin{aligned} \begin{Bmatrix} N_{xx} \\ N_{yy} \\ N_{xy} \end{Bmatrix} &= \begin{bmatrix} A_{11} & A_{12} & A_{16} \\ A_{21} & A_{22} & A_{26} \\ A_{61} & A_{62} & A_{66} \end{bmatrix} \begin{Bmatrix} \epsilon_{xx}^\circ \\ \epsilon_{yy}^\circ \\ \gamma_{xy}^\circ \end{Bmatrix}, \\ \begin{Bmatrix} M_{xx} \\ M_{yy} \\ M_{xy} \end{Bmatrix} &= \begin{bmatrix} D_{11} & D_{12} & D_{16} \\ D_{21} & D_{22} & D_{26} \\ D_{61} & D_{62} & D_{66} \end{bmatrix} \begin{Bmatrix} \kappa_{xx} \\ \kappa_{yy} \\ \kappa_{xy} \end{Bmatrix}. \end{aligned} \quad (8)$$

⁸⁷⁸ If we make the simplifying assumptions [32, 33] that
⁸⁷⁹ (1) the laminate experiences pure axial loading and trans-
⁸⁸⁰ verse bending (i.e., $N_{yy} = N_{xy} = 0$ and $M_{yy} = M_{xy} = 0$,
⁸⁸¹ respectively), and (2) the laminate is a beam of suffi-
⁸⁸² ciently high aspect ratio to minimize the Poisson effect
⁸⁸³ and anisotropic shear coupling (i.e., below we effectively

884 let $A_{12}^* = A_{16}^* = 0$ and $D_{12}^* = D_{16}^* = 0$), then we can
 885 calculate the in-plane effective flexural and axial Young's
 886 moduli of the laminate along the x-axis.

887 For axial Young's modulus of the laminate, we first
 888 define the average membrane stresses in the laminate as:

$$\{\bar{\sigma}^m\} = \frac{\{N\}}{z_1 - z_n}. \quad (9)$$

889 By substitution in Eq. 7, we obtain:

$$\begin{Bmatrix} \bar{\sigma}_{xx}^m \\ \bar{\sigma}_{yy}^m \\ \bar{\tau}_{xy}^m \end{Bmatrix} = \frac{1}{(z_1 - z_n)} \begin{bmatrix} A_{11} & A_{12} & A_{16} \\ A_{21} & A_{22} & A_{26} \\ A_{61} & A_{62} & A_{66} \end{bmatrix} \begin{Bmatrix} \epsilon_{xx}^m \\ \epsilon_{yy}^m \\ \gamma_{xy}^m \end{Bmatrix}, \quad (10)$$

890 and, by inverting this equation (let $A^* = A^{-1}$) and
 891 substituting $A_{12}^* = A_{16}^* = 0$ based on the assumptions
 892 above, we infer:

$$\epsilon_{xx}^m = (z_1 - z_n) A_{11}^* \bar{\sigma}_{xx}^m. \quad (11)$$

893 We therefore define Young's modulus for effective axial
 894 elasticity as:

$$E_{xx}^m = \frac{\bar{\sigma}_{xx}^m}{\epsilon_{xx}^m} = \frac{1}{(z_1 - z_k) A_{11}^*}. \quad (12)$$

895 To find the transverse flexural Young's modulus of the
 896 laminate, we first specify the moment-curvature relation
 897 of an Euler-Bernoulli beam:

$$M = EI\kappa. \quad (13)$$

898 Along the x-axis, the second moment of area for a
 899 rectangular cross-section is:

$$I_{yy} = \frac{b(z_1 - z_n)^3}{12}. \quad (14)$$

900 Given the assumption that $M_{yy} = M_{xy} = 0$, the mo-
 901 ment along the x-axis is related to the moment of the
 902 beam by:

$$M = M_{xx}b. \quad (15)$$

903 Thus, given the assumption that $D_{12}^* = D_{16}^* = 0$,
 904 Young's modulus for the effective transverse flexural elas-
 905 ticity of the laminate can be found by making Eq. 13
 906 specific to transverse flexure of the x-axis and rearranging
 907 the terms:

$$E_{xx}^f = \frac{12M_{xx}}{(z_1 - z_n)^3 \kappa_{xx}}. \quad (16)$$

908 From inversion of Eq. 7 (let $D^* = D^{-1}$), this reduces
 909 to:

$$E_{xx}^f = \frac{12}{(z_1 - z_n)^3 D_{11}^*}. \quad (17)$$

Statistical analysis

911 *Model selection and fitting.* In order to explore the
 912 relationships between the composite structure and me-
 913 chanical properties of the cuticle, we fit phylogenetic
 914 linear mixed-effects models (PGLMM) to the tensile
 915 testing data using maximum likelihood estimation [48–
 916 51]. Raw data was processed using a custom script in
 917 Python version 3.5.2 [52]. Model exploration and fitting
 918 was conducted in R version 3.5.1 (2018-07-02) --
 919 “Feather Spray”, using the ‘nlme’ and ‘ape’ pack-
 920 ages [53–55]. Response variables and covariates were
 921 natural-log transformed, as needed, to ensure that the
 922 normalized model residuals were normally distributed
 923 [R:shapiro.test] and homoscedastic [R:levene.test],
 924 using numerical and graphical analysis. In order to con-
 925 trol for phylogenetic non-independence in the data, we
 926 included the species of each specimen as a random ef-
 927 fect in all models. We also allowed for correlation in
 928 the error term of the models, as specified by a variance-
 929 covariance matrix generated from a Brownian motion
 930 model of trait evolution [R:‘ape’:corBrownian] along a
 931 phylogeny [54, 56].

932 The preferred phylogeny for select North American *Cur-*
933 culio species is that of Bonal et al. [35]. This phylogeny
934 was generated using Maximum-Likelihood methods; it is
935 untrametric yet has uniform internal branch lengths. The
936 preferred tree was pruned to include only those species
937 used in tensile testing, with a polytomy at each species’
938 root node to represent the individual specimens examined
939 for that species. Because the branch lengths of the tree
940 were not specified, all branch lengths were set equal to 1.
941 Underestimation of branch lengths causes overestimation
942 of phylogenetic signal [56–58]. We were unable to detect
943 statistically significant phylogenetic signal for any of our
944 models. For this reason we consider our study’s principal
945 findings to be unaffected by branch length underestima-
946 tion. However, because of the relatively poor taxonomic
947 resolution afforded by a sample of five species, we are
948 unable to conclude whether significant phylogenetic signal
949 exists in the traits examined herein.

950 Other models of trait evolution were considered dur-
 951 ing model exploration; including Ornstein-Uhlenbeck
 952 [R:‘ape’:corMartins] and variable rate (AC/DC) mod-
 953 els [R:‘ape’:corBlomberg] [54, 56]. These models were
 954 chosen to compare among competing hypotheses of trait
 955 evolution, namely stabilizing selection and variable-rate
 956 evolution, respectively. We additionally tested a Brownian
 957 motion model of trait evolution, corresponding to varia-
 958 tion constrained by clade membership (i.e., sister taxa are
 959 more similar to each other than to an out-group). How-
 960 ever, neither of the former produced a significantly better
 961 fit to the data than the Brownian motion model for any
 962 comparison, as measured by likelihood score and residual
 963 variance; viz. R_σ^2 , and $R_{\beta^*}^2$ [R:‘r2glmm’:r2beta]. R_σ^2
 964 is the proportion of generalized variance explained by
 965 fixed effects. This measure is generally used for compar-
 966 ison of covariance structures [59–61]. $R_{\beta^*}^2$ measures the

multivariate association between the outcome and the of endocuticle produced a significant fixed effect. We fixed effects within a given correlation structure, and is therefore elected to make the model more parsimonious generally used to compare fixed effects [59–61]. Using by removing cross-sectional area of exocuticle as a fixed the R package ‘phytools’ [56, 62], we also estimated the effect. The final model generated for our first aim featured phylogenetic signal in the residual variance of each model; the ratio of exocuticle to endocuticle in cross-section as a taking into account two measures of spatial autocorrelation fixed effect, with ultimate tensile strength as the response (Abouheif’s \bar{C} and Moran’s I), and two measures of variable.

phylogenetic signal (Pagel’s λ and Blomberg’s κ).

In all models, we tested whether the inclusion of phylogenetic correlation in the model error produced significantly better model fit, using a likelihood-ratio test [R: ‘lmtree’:‘lrtest’] and R^2 -difference test [R: ‘r2glmm’:‘r2beta(method=‘sgv’)] between the fully-specified model and a model lacking the phylogenetic effect [61, 63]. Models that incorporated covariance due to Brownian motion consistently produced higher likelihood scores and fit to the data. However, no model exhibited statistically significant phylogenetic signal in any of the variables. Our findings imply that *residual*

variance in the examined traits does not exhibit significant rate-variation or stabilizing selection in the amount or direction of residual variance between groups; rather, variation within and between clades is distributed randomly by clade, with limited phylogenetic dependence. Once models were fitted to the data, T- and F-statistics were calculated to determine whether each cofactor was significantly different from zero.

Hypothesis testing. Our objectives for hypothesis testing using the PGLMMs were threefold: (1) to assess whether the altered ratio of exocuticle to endocuticle in the rostral apex has an effect on the tensile strength of the rostrum; (2) to test whether a trade-off exists between specimen stiffness and resistance to fracture; and (3) to examine whether rostrum length and flexibility are correlated.

To test the relationship between relative layer thicknesses and tensile strength, we fitted a fully-specified model with the cross-sectional area of exocuticle and endocuticle at the site of fracture as fixed effects, including an interaction term, and with the maximum tensile force sustained prior to fracture as a response variable. This model was then compared to models with only cross-sectional area of either endocuticle or exocuticle, but not both, as the sole fixed effect in the model. We then tested whether one or both regions were significantly correlated in a likelihood-ratio test and $R^2_{\beta^*}$ -difference test between each of the three models. Only the cross-sectional area

For our second aim we examined the relationship between specimen stiffness and resistance to fracture. Specimen stiffness was characterized using a low strain elastic modulus – averaged across the first 33% of the stress-strain curve – and the secant modulus at failure. Resistance to fracture was quantified in terms of ultimate strain and work of fracture, measured as area under the stress-strain curve. Four models were fitted, two of which had ultimate strain as the response variable, and two with work of fracture as response variable. Each model then used one of the different measures of specimen stiffness as a fixed effect.

Finally, for the third aim we explored whether a size-effect might exist in the *Curculio* rostrum; and specifically if longer and typically more curved rostra were more flexible than shorter, straighter rostra. We generated two models; the low strain and secant elastic moduli individually served as response variables, with specimen length as the fixed effect in both.

Code availability

R, Python, and Matlab scripts used to manipulate and analyze the raw data and processed data, produce figures, and estimate effective elastic constants are provided in Supplement 1.

Data availability

Stress-strain curves for all tensile and fatigue-tested specimens are provided as PDFs (Supplement 2). Diagnostic plots for all PGLMMs are provided as PDFs (Supplement 3). PGLMM terms and output are provided (Supplement 4). All measurements used for related to the maximum force sustained in tension, using PGLMM generation are provided as a CSV file (Supplement 5). Raw and processed data will be provided by the corresponding author upon reasonable request.

REFERENCES

- 1055
- 1056 [46] Arnett Jr., R. H., Samuelson, G. A., and Nishida G. M. *The Insect and Spider Collections of the World, 2nd Edition.* Fauna and Flora Handbook No. 11. (Sandhill Crane Press, Gainesville, 1993).
- 1057
- 1058
- 1059
- 1060 [47] The MathWorks, Inc., *MATLAB and Statistics Toolbox* (Natick, Mass., Release R2018b, 2018).
- 1061
- 1062 [48] Galecki, A. and Burzykowski, T. *Linear Mixed-Effects Models Using R. A Step-by-Step Approach* (Springer, New York, 2013).
- 1063
- 1064
- 1065 [49] Hadfield, J. D. and Nakagawa, S. General quantitative genetic methods for comparative biology: phylogenies,
- 1066

- 1067 taxonomies and multi-trait models for continuous and cat- 1086 [56] Münkemüller, T. et al. How to measure and test phylo-
 1068 egorical characters *J. Evol. Biol.* **23:3**, 494–508, (2010). 1087 netic signal *Methods Ecol. Evol.* **3:4**, 743–756, (2012).
- 1069 [50] Housworth, E. A., Martins, E. P., and Lynch, M. The Phy- 1088 [57] Stone, E. A. Why the phylogenetic regression appears
 1070 logenetic Mixed Model *Am. Nat.* **163:1**, 84–96, (2004). 1089 robust to tree misspecification *Syst. Biol.* **60:3**, 245–260,
 1071 [51] Stone, G. N., Sean, N., and Felsenstein, J. Controlling 1090 (2011).
- 1072 for non-independence in comparative analysis of patterns 1091 [58] Molina-Venegas, R. and Rodríguez, M. Á. Revisiting phy-
 1073 across populations within species *Philos. Trans. Royal 1092 logenetic signal; strong or negligible impacts of polytomies
 1074 Soc. B* **366:1569**, 1410–1424, (2011). 1093 and branch length information? *BMC Evol. Biol.* **17:1**,
 1075 [52] Python Core Team. *Python: A dynamic, open source pro- 1094 1–53, (2017).*
- 1076 gramming language (Python Software Foundation, Version 1095 [59] Nakagawa, S. and Schielzeth, H. A general and simple
 1077 3.5.2, 2018). 1096 method for obtaining R² from generalized linear mixed-
 1078 [53] R Development Core Team *R: A Language and Environ- 1097 effects models* *Methods Ecol. Evol.* **4:2**, 133–142, (2013).
- 1079 ment for Statistical Computing
- 1080 (R Foundation for Statistical Computing, Vienna, Version 3.5.1, 2008). 1098 [60] Jaeger, B. C., Edwards, L. J., Das, K., and Sen, P. K.
 1081 [54] Paradis, E. and Schliep, K. ape 5.0: an environment for 1099 An R² statistic for fixed effects in the generalized linear
 1082 modern phylogenetics and evolutionary analyses in R 1100 mixed model *J. Appl. Stat.* **44:6**, 1086–1105, (2016).
- 1083 *Bioinformatics* **5:0**, (2018). 1101 [61] Jaeger, B. Computes R Squared for Mixed (Multilevel)
 1084 [55] Pinheiro, J. et al. nlme: Linear and Nonlinear Mixed 1102 Models **Version 0.1.2** (2017).
- 1085 Effects Models **R package version 3.1-137**, (2018). 1103 [62] Liam, J. R. phytools: An R package for phylogenetic
 1086 1104 comparative biology (and other things) *Methods Ecol.*
 1087 and *Evol.* **3**, 217–223, (2012).
- 1088 1105 [63] Zeileis, A. and Hothorn, T. Diagnostic Checking in Re-
 1089 gression Relationships *R News* **2:3**, 7–10, (2002).
- 1090 1106 [64] R Core Team. *R: A Language and Environment for Statistical Computing* (R Foundation for Statistical Computing, Vienna, Austria, Version 3.6.1, 2019).
- 1091 1107